

Color–selected galaxies at $z \approx 6$ in the Great Observatories Origins Deep Survey ¹

M. Dickinson², D. Stern³, M. Giavalisco², H. C. Ferguson², Z. Tsvetanov⁴, R. Chornock⁵,
S. Cristiani⁶, S. Dawson⁵, A. Dey⁷, A. V. Filippenko⁵, L. A. Moustakas², M. Nonino⁶, C.
Papovich⁸, S. Ravindranath², A. Riess², P. Rosati⁹, H. Spinrad⁵, E. Vanzella^{9,10}

ABSTRACT

We report early results on galaxies at $z \sim 6$, selected from *Hubble Space Telescope* imaging for the Great Observatories Origins Deep Survey. Spectroscopy of one object with the Advanced Camera for Surveys grism and from the Keck and VLT observatories shows a strong continuum break and asymmetric line emission, identified as Ly α at $z = 5.83$. We detect only five spatially extended, $z \sim 6$ candidates with signal-to-noise ratios > 10 , two of which have spectroscopic confirmation. This is many fewer than would be expected if galaxies at $z = 6$ had the same luminosity function as those at $z = 3$. There are many fainter candidates, but we expect substantial contamination from foreground interlopers and spurious detections. Our best estimates favor a $z = 6$ galaxy population

¹Based on observations taken with the NASA/ESA Hubble Space Telescope, which is operated by AURA, Inc., under NASA contract NAS5–26555; from the W. M. Keck Observatories; and from the Very Large Telescope (VLT) at Cerro Paranal, Chile, operated by the European Southern Observatory, under programs 170.A-0788 and 168.A-0485.

²Space Telescope Science Institute (STScI), 3700 San Martin Dr., Baltimore, MD 21218.

³Jet Propulsion Laboratory, California Institute of Technology, Mail Stop 169-506, Pasadena, CA 91109

⁴Department of Physics and Astronomy, The Johns Hopkins University, 3400 N. Charles St., Baltimore, MD 21218–2686

⁵Department of Astronomy, University of California, Berkeley, Mail Code 3411, Berkeley, CA 94720

⁶Istituto Nazionale di Astrofisica, Osservatorio Astronomico di Trieste, via G.B. Tiepolo 11, Trieste, I-34131, Italy

⁷National Optical Astronomical Observatory, 950 North Cherry Avenue, Tucson, AZ 85719

⁸Steward Observatory, University of Arizona, 933 Cherry Ave., Tucson, AZ 85721–0065

⁹European Southern Observatory, Karl–Schwarzechild–Strasse 2, D–85748 Garching bei München, Germany

¹⁰Dipartimento di Astronomia dell’Università di Padova, Vicolo dell’Osservatorio 2, I-35122 Padova, Italy

with fainter luminosities, higher space density, and similar co-moving ultraviolet emissivity to that at $z = 3$, but this depends critically on counts at fluxes fainter than those reliably probed by the current data.

Subject headings: early universe — galaxies: high-redshift – galaxies: formation
– galaxies: evolution

1. Introduction

Broad band color selection, based on ultraviolet (UV) spectral breaks caused by neutral hydrogen, is an efficient technique for identifying galaxies at $z = 3$ to 4 with imaging from the ground and from the *Hubble Space Telescope* (Steidel et al. 1996; Madau et al. 1996). At higher redshifts and relatively bright magnitudes, $i' - z'$ colors from the Sloan Digital Sky Survey have been used to identify QSOs out to $z = 6.4$ (Fan et al. 2003). Some galaxies at $z > 5$ have also been found in this way, but the required deep imaging and spectroscopy is extremely challenging. A Lyman break galaxy (LBG) with typical (L^*) UV luminosity at $z = 3$ ($M_{1700\text{\AA}} = -21.0$, Adelberger & Steidel 2000) would have $m(z) = 26.0$ if moved, without evolution, to $z = 6$, and would be undetected in the i -band (hence, an “ i -dropout”). At $z \gtrsim 6.5$, $\text{Ly}\alpha$ shifts through the z -band, and galaxies are lost to optical sight altogether.

One goal of the Great Observatories Origins Deep Survey (GOODS) is to find and study large numbers of galaxies at $3.5 < z < 6.5$. Here, we report initial results from GOODS on galaxy candidates at $z \sim 6$, including spectroscopy for one galaxy, CDFS J033240.0–274815 (henceforth SiD2), with the ACS grism and the Keck and VLT observatories. We use AB magnitudes ($\text{AB} \equiv 31.4 - 2.5 \log \langle f_\nu / \text{nJy} \rangle$), and assume a cosmology with $\Omega_{\text{tot}}, \Omega_M, \Omega_\Lambda = 1.0, 0.3, 0.7$ and $H_0 = 70 \text{ km s}^{-1} \text{ Mpc}^{-1}$.

2. Imaging, photometry, and color-selection

The GOODS Treasury program covers areas around the Chandra Deep Field South (CDF-S) and Hubble Deep Field North (HDF-N) with mosaics of ACS images. The observations, data reduction, and catalogs are described in Giavalisco et al. (2003a). Our present analysis uses 3-epoch co-added images for both fields, with 3, 1.5, 1.5 and 3 orbit depth in the F435W, F606W, F775W, and F850LP filters (henceforth B_{435} , V_{606} , i_{775} , and z_{850}). After discarding regions near the image borders or without 4-band coverage, the survey solid angle is 316 arcmin^2 . We detect objects in the z_{850} images using SExtractor (Bertin & Arnouts 1996), and measure photometry through matched apertures in all bands. Here,

we use z_{850} “total” magnitudes (SExtractor MAG_AUTO), and colors measured through isophotal apertures defined in the z_{850} image.

We estimate the reddest colors expected for ordinary galaxies with spectral templates (Coleman, Wu & Weedman 1980) integrated through the ACS bandpasses. The redshifted colors of an elliptical galaxy peak¹¹ at $i_{775} - z_{850} \approx 1.2$ for $z \approx 1.1$. There is only one “bright” galaxy in the GOODS fields with $i_{775} - z_{850} > 1.3$ ($z_{850} = 23.9$; $i_{775} - z_{850} = 1.32$). It is well detected at V_{606} , bright in the near-infrared (IR), and certainly has $z \ll 6$. Redder colors may be explained by dust obscuration, high metallicity, strong line emission in the z_{850} -band, or intergalactic medium (IGM) absorption at high redshift. For the range of intrinsic UV colors seen for LBGs at $z \approx 3$, $i_{775} - z_{850} > 1.3$ is crossed at $z = 5.5$ to 5.7 . Cool stellar dwarfs may also be this red. Fan et al. (2003) Figure 2 shows that only a tiny minority of high-latitude stars have $i' - z' > 1.3$, and our ACS imaging provides a robust measure of stellarity for $z_{850} < 26.2$.

Our current ACS mosaics have very small misalignments between images from different observing epochs. These can trigger over-rejection in the cores of point sources during cosmic ray removal in the V_{606} and i_{775} bands (only – the B_{435} and z_{850} images are reduced differently). There is virtually no photometric impact for extended sources (Giavalisco et al. 2003a), but the $i_{775} - z_{850}$ colors of brighter stars can be biased redward, and we treat them with caution here.

We are interested in objects near our detection limits. The signal-to-noise ratio (S/N) of a measurement depends on the source flux and size, and on the exposure time, which varies with position in our mosaics. The significance of a source is best estimated not from its magnitude, but from $S/N(z_{850})$ in the detection aperture. Our photometric errors are computed from noise maps which account for inter-pixel correlations. To verify their reliability, we added artificial objects to the z_{850} images (only) and detected them with SExtractor. Background-subtracted counts (S_i) were measured through matched apertures for the other bands, and compared to the predicted uncertainties (σ_i) from the noise maps. The distribution of S_i/σ_i is nearly Gaussian with mode ≈ 0 and RMS ≈ 1 , showing that our error estimates are reliable, except for a positive tail due to blending with other objects. Because of this tail, 14% of $z \sim 6$ galaxies would have $S/N > 2$ in the B_{435} or V_{606} bands.¹² We consider this an acceptable loss rate, and adopt $i_{775} - z_{850} > 1.3$ and $S/N(B_{435}, V_{606}) < 2$ as our i -dropout criteria (Figure 1).

¹¹The redshifted elliptical template has redder colors at $1.7 < z < 2.3$, but the UV spectrum of any galaxy at that redshift is unlikely to resemble that of an old elliptical at $z \approx 0$.

¹²On average, this limit corresponds to B_{435} or $V_{606} > 29.1$.

3. Spectroscopy

Supernovae found in GOODS ACS imaging are studied in a target-of-opportunity program which, in some cases, obtains low-resolution, slitless spectra with the ACS G800L grism. One grism observation (SN2002FW, Riess et al. (2003)) included SiD2, which we had noted as an *i*-dropout candidate. The data were obtained on UT 2002 October 01, with an exposure time of 18840s, and were reduced with the `calacs` pipeline and the `aXe` extraction software. The G800L spectrum (Figure 2a) shows a flat continuum with a sharp break at $\lambda \approx 8300\text{\AA}$, explaining the red $i_{775} - z_{850}$ color.

We observed SiD2 with the Low Resolution Imaging Spectrometer (LRIS; Oke et al. (1995)) on the Keck II telescope on UT 2002 October 09 in poor weather conditions, but detected line emission at 8303\AA . Deeper observations (7.8 ks of integration) with the 400 lines mm^{-1} grating ($\lambda_{\text{blaze}} = 8500\text{\AA}$; $R \approx 1000$) were obtained on UT 2002 November 08. Observations (12 ks) with the Focal Reducer/Low Dispersion Spectrograph (FORS2) on the Yepun telescope (VLT 4) were obtained on UT 2002 December 08 with the 300I grism ($R \approx 860$). We reduced the data with IRAF following standard procedures, and combined the LRIS and FORS2 data with appropriate weighting. The final spectrum (Figure 2b) shows $\text{Ly}\alpha$ emission at $z = 5.829$ with flux $1.6 \times 10^{-17} \text{ erg cm}^{-2} \text{ s}^{-1}$. The line shows the blue cut-off characteristic of high-redshift $\text{Ly}\alpha$ emitters, and the $\text{Ly}\alpha$ forest continuum break is clearly evident. The emission line is not obviously detected in the grism spectrum. The ACS exposure time calculator predicts a line detection with $S/N \approx 15$ for a point source. Extended line emission superimposed on the galaxy continuum, however, is evidently invisible.

We also obtained a spectrum of the only spatially extended HDF-N candidate with $S/N(z_{850}) > 10$ (J123619.9+620934) with Keck/LRIS on UT 2003 May 01, but did not successfully measure a redshift.

4. Other candidate $z \approx 6$ objects

There are 16 objects with $S/N(z_{850}) > 10$ that meet our selection criteria. 11 are point sources (3.4% of the stellar objects with $24 < z_{850} < 26.2$; $0''.12 < \text{FWHM} < 0''.16$ versus $0''.18$ – $0''.7$ for the other $S/N > 10$ candidates), whose $i_{775} - z_{850}$ colors are suspect (§2). The GOODS project has gathered deep near-IR imaging with the VLT ISAAC camera covering $\sim 30\%$ of our CDF-S field (Giavalisco et al. 2003a), including all three CDF-S stellar *i*-dropout candidates. Their $z_{850} - J$ colors are too red compared to expectations for high-redshift objects (Figure 3). Although some of the 8 HDF-N point sources might

conceivably be high redshift objects, we believe that they are probably stars and will not consider them further here. This leaves five extended $z \sim 6$ candidates, or 0.016 arcmin² (Table 1).

Stanway, Bunker & McMahon (2003, SBM) used the public release v0.5 GOODS ACS CDF–S data to identify nine i –dropout candidates. Three are in our sample, and two have been confirmed spectroscopically (Bunker et al. 2003, this paper). SBM#5 (J033238.80–274953.6) is unresolved, with the reddest $i_{775} - z_{850}$ color (> 2.7 at 2σ) of any GOODS object. Its exceptionally blue near–IR colors ($J - H = -0.3$, $H - K = -0.5$, AB) suggest that it may be a T–dwarf (see also SBM). Another point source, SBM#4, was observed in the GOODS spectroscopic program and is a cool star (approximately L0V). SBM#2, 4, 8 and 9 have $S/N > 2$ in V_{606} and/or B_{435} , are fairly bright in near–IR images, and are thus unlikely to be at $z \sim 6$. SBM#6 falls outside the area analyzed here, where the Viz data are shallow and there are no B_{435} data. In summary, three (perhaps four) of the nine SBM objects are good $z \sim 6$ candidates.

Data artifacts (space junk trails, reflection ghosts, diffraction spikes, residual cosmic rays) can produce spurious z_{850} detections without shorter–wavelength counterparts which mimic i –dropouts. We have removed most of these by visual inspection. This is generally easy at $S/N > 10$, but this corresponds to $\langle z_{850} \rangle \approx 25.3$, which is fairly bright for galaxies at $z \approx 6$. Our catalogs push deeper; *post–facto*, we truncate them at $S/N \geq 5$ and reject sources that are too small or sharp to be real. Even after careful inspection, however, some spurious sources probably remain. As one check, we masked areas with objects, inverted the images, and detected “negative sources.” We find 57 which qualify as i –dropouts. All have $-S/N < 8$, and $\sim 75\%$ have $5 < -S/N < 6$.

The vast majority of real, faint galaxies have $i_{775} - z_{850} < 1.3$ and $z \ll 6$, but measurement errors may scatter a small fraction to redder colors. We estimate this contamination using brighter objects ($S/N(z_{850}) > 20$). We randomly assign their colors to fainter objects, then perturb the simulated fluxes using the error distributions quantified in §2. Only ~ 2 foreground interlopers with $S/N > 10$ would (barely) meet the i –dropout criteria, while ~ 49 objects with $5 < S/N < 10$ could do so.

Together, these contaminants represent $< 0.7\%$ of the ~ 16000 GOODS sources with $5 < S/N(z_{850}) < 10$, but may contribute $\sim 45\%$ of the faint $z \sim 6$ candidates. After subtracting the expected contamination, we estimate that there are ~ 145 candidates with $S/N > 5$ (0.46 arcmin^{−2}), $> 50\%$ of which have $5 < S/N < 6$.

There are four extended candidates with $S/N > 7$ in the portion of the CDF–S with deep ISAAC imaging (Figure 3). One has red $z_{850} - J$ and bright IR magnitudes, and is

unlikely to be at $z \approx 6$. Two or perhaps three candidates, including SiD2, are very faint in the near-IR ($24.7 < J_{AB} < 24.9$), with colors expected for galaxies at $5.5 < z < 6$.

5. Discussion

The $i_{775} - z_{850}$ color limit sets a lower redshift bound for i -dropouts, while IGM suppression in z_{850} makes the upper bound, and hence the sampling volume, a strong function of luminosity. We use simulations (Giavalisco et al. 2003b) to predict number counts of candidates, including photometric biases. We generated artificial galaxies with a mixture of disk and bulge surface brightness profiles, ellipticities, and orientations. Their sizes were drawn from a log-normal distribution tuned to reproduce measurements at $z \approx 3$ –5 (Ferguson et al. 2003). Their spectra have a distribution of UV spectral slopes that matches the observed colors of LBGs at $z \approx 3$ (Adelberger & Steidel 2000). We distributed the galaxies in redshift, modulated their spectra by IGM opacity (Madau 1995), convolved them with ACS point spread functions, added them to the GOODS images at various magnitudes, and recovered them with SExtractor.

Figure 4 compares the number of i -dropout candidates to simulations for various assumptions about the UV luminosity function (LF), which we model as a Schechter (1976) distribution with a faint-end slope fixed to $\alpha = -1.6$, as measured for LBGs at $z = 3$ (Adelberger & Steidel 2000). The number of *bright* galaxies is smaller at $z \approx 6$ than at $z = 3$ (see also SBM; Bremer & Lehnert 2003 find a similar result from ground-based imaging for LBGs at $z \approx 5.3$). The $z = 3$ LF is excluded with a high degree of confidence ($P < 10^{-8}$). It predicts 30 galaxies with $S/N(z_{850}) > 10$ vs. 5 observed, and 26 with $z_{850} < 25$ vs. ≤ 7 observed.¹³ A change in the number of bright objects does not require comparable evolution in the total luminosity density of the population; the number of bright sources is exponentially sensitive to the value of L^* . Schechter functions fit to the counts in Fig. 4a favor fainter L^* and higher ϕ^* compared to their values at $z = 3$. Integrating acceptable fits for $M_{1700\text{\AA}} < -19.4$ ($\approx 0.2L_{z=3}^*$), the UV emissivity is similar to that at $z = 3$ ($\rho(L_{z=6})/\rho(L_{z=3}) = 0.77^{+0.29}_{-0.23}$, 95.4% confidence). However, these fitted L^* values, and hence most of the inferred luminosity density, are at $z_{850} > 26.4$, where the current data are most uncertain. The LF fit is strongly driven by objects with $5 < S/N < 6.3$ (Fig. 4b). A model with $L_{z=6}^* = L_{z=3}^*$ and $5\times$ smaller ϕ^* (and ρ_L) is consistent with the data at brighter magnitudes and higher S/N ratios, but drastically underpredicts the counts at low S/N and $z_{850} > 25.5$. Fits excluding

¹³Out of 7 candidates with $z_{850} < 25$, only one has $S/N(z_{850}) > 10$. The others may be real, but contamination may be substantial.

the lowest S/N bin leave the total ρ_L essentially unconstrained. A robust determination of the $z = 6$ LF and total emissivity requires data significantly deeper than those used here.

Two other studies have analyzed i -dropouts from somewhat deeper ACS images. Yan, Windhorst & Cohen (2003) found 2.3 candidates/arcmin² with $S/N(z_{850}) > 7.2$ in an ACS field with exposure time $1.5\times$ longer in z_{850} than the 3-epoch GOODS data, but $4.9\times$ longer in i_{775} , thus providing more robust color discrimination against interlopers. Their density is $10\times$ larger than ours to the same S/N threshold. They estimate their catalogs are 100% complete for $z_{850} \leq 28.0$, whereas ours are only 50% complete for point sources at $z_{850} = 26.7$ (Giavalisco et al. 2003a). Yan et al. may have underestimated their source fluxes or spurious detection rate, but it is notable that they also find very few bright candidates (none with $z_{850} < 26.8$). Bouwens et al. (2003) identified 0.5 candidates/arcmin² with $z_{850} < 27.3$ from imaging (5–20 orbits in z_{850}) covering 46 arcmin². They also find few bright candidates (only one with $z_{850} < 25.5$), and estimate $\rho(L_{z=6})/\rho(L_{z=3}) = 0.6 \pm 0.2$.

In summary, we have identified five spatially extended, high- S/N candidates for galaxies at $z \sim 6$ in early GOODS ACS imaging. Two have confirmed redshifts $z \approx 5.8$. There are many fainter candidates, but we estimate that $\sim 45\%$ may be spurious detections or foreground interlopers. The number of robust candidates is smaller than is predicted if the LF were the same as that at $z \approx 3$. Our best estimates find fainter L^* , larger ϕ^* , and moderately smaller ρ_L compared to $z = 3$, but this strongly depends on the number of objects at $z_{850} > 26$, which is as yet poorly measured. Constant L^* with smaller ϕ^* and ρ_L are consistent with the bright counts but greatly underpredict the number of faint sources. The measurements do not require (nor robustly exclude) a dramatic change in ρ_L from $z \sim 6$ to 3, especially if L^* is evolving with redshift. Giavalisco et al. (2003b) find only a modest change ($-30\% \pm 10\%$) in the luminosity density from $z = 3$ to $z \approx 5$ where the GOODS LBG sample is much better characterized. Our best estimates are consistent with an extrapolation of those results to $z = 6$, but deeper data are needed for a robust measurement. The final GOODS images will be deeper, with fewer contaminating artifacts. This, together with much deeper data (e.g., the forthcoming ACS Ultradeep Field), will provide better constraints on the galaxy population at these highest optically-accessible redshifts.

We thank the members of the GOODS team, and the staff at STScI, ESO and the Keck Observatory, who made this project possible. Support was provided by NASA through grant GO09583.01-96A from STScI, which is operated by AURA under NASA contract NAS5-26555. Work by LM and DS was supported by NASA through the *SIRTF* Legacy Science Program, through contract number 1224666, issued by JPL, California Institute of Technology, under NASA contract 1407.

REFERENCES

- Adelberger, K. L., & Steidel, C. C., 2000, *ApJ*, 544, 218
- Bertin, E., & Arnouts, S. 1996, *A&AS*, 117, 393
- Bremer, M., & Lehnert, M. D., 2003, *ApJ*, in press
- Bouwens, R. J., et al., 2003, *ApJ*, in press
- Bunker, A. J., Stanway, E. R., Ellis, R. S., McMahon, R. G., & McCarthy, P. J., 2003, *MNRAS*, submitted
- Coleman, G. D., Wu, C.-C., & Weedman, D. W. 1980, *ApJS*, 43, 393
- Ferguson, H. C., et al., 2003, *ApJ Letters*, submitted
- Fan, X., et al., 2003, *AJ*, 125, 1649
- Giavalisco, M., et al., 2003a, *ApJ Letters*, submitted
- Giavalisco, M., et al., 2003b, *ApJ Letters*, submitted
- Madau, P., 1995, *ApJ*, 441, 18
- Madau, P., Ferguson, H. C., Dickinson, M., Giavalisco, M., Steidel, C. C., & Fruchter, A. 1996, *MNRAS*, 283, 1388
- Oke, J. B., et al., 1995, *PASP*, 107, 375
- Riess, A., et al., 2003, *ApJ Letters*, submitted
- Schechter, P., 1976, *ApJ*, 203, 297
- Stanway, E. R., Bunker, A. J., & McMahon, R. G., 2003, *MNRAS*, in press
- Steidel, C. C., Giavalisco, M., Pettini, M., Dickinson, M., & Adelberger, K. L. 1996, *ApJ*, 462, L17
- Yan, H., Windhorst, R. A., & Cohen, S. H., 2003, *ApJ*, 585, L93

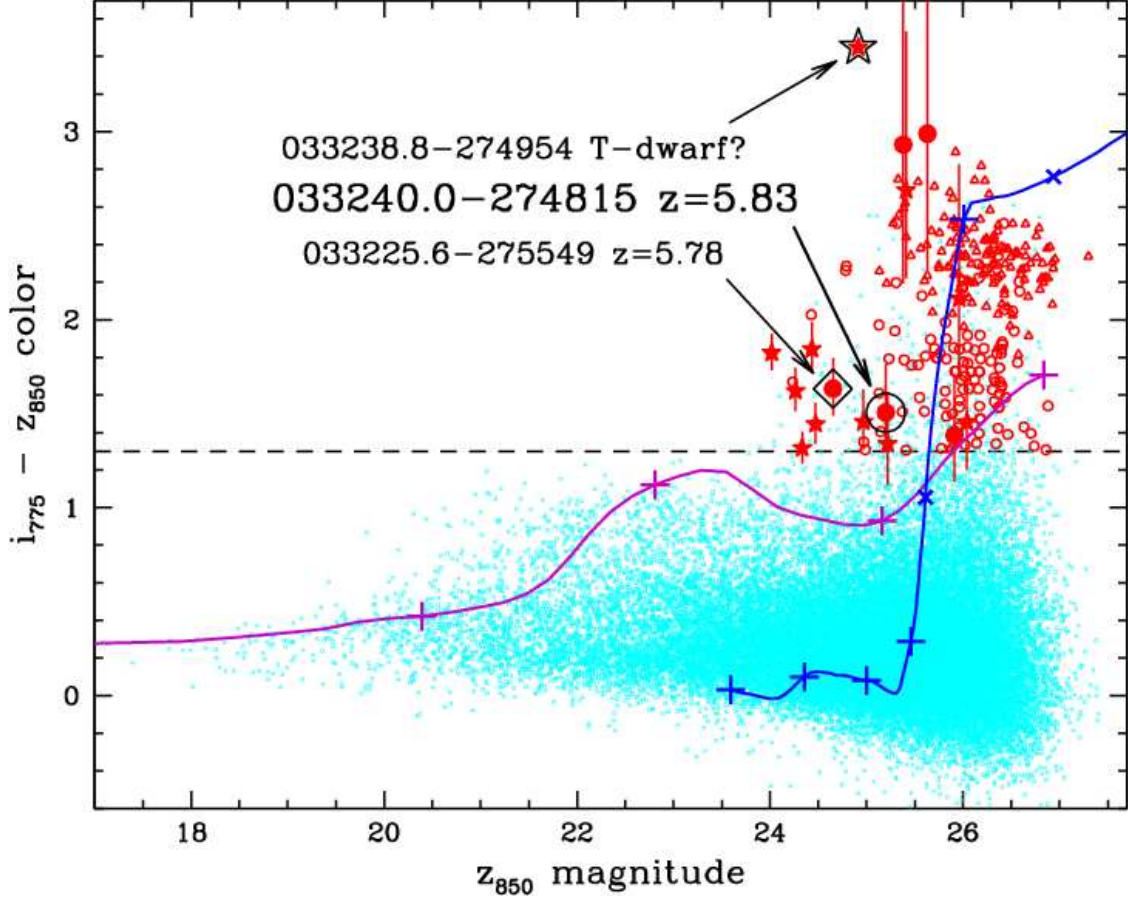


Fig. 1.— Color-magnitude diagram for the GOODS CDF-S + HDF-N fields. The dashed line shows our i -dropout color selection limit. Light blue points are extended objects that do not meet the color and $S/N(B_{435}, V_{606}) < 2$ criteria. Triangles mark 1σ lower color limits for objects undetected in i_{775} . Red points are i -dropout candidates. Larger, filled points with error bars (1σ) are candidates with $S/N(z_{850}) > 10$; stars mark point sources. Two galaxies with spectroscopic redshifts are highlighted, as is a possible T-dwarf. The mauve curve shows the color-magnitude track for an unevolving, L^* elliptical galaxy; vertical crosses mark $z = 0.5, 1, 1.5$ and 2.0 . The blue curve shows the track for an unevolving $L^*_{z=3}$ LBG with average UV colors; vertical crosses mark $z = 2, 3, 4, 5$, and 6 , while tilted crosses mark $z = 5.5$ and 6.5 .

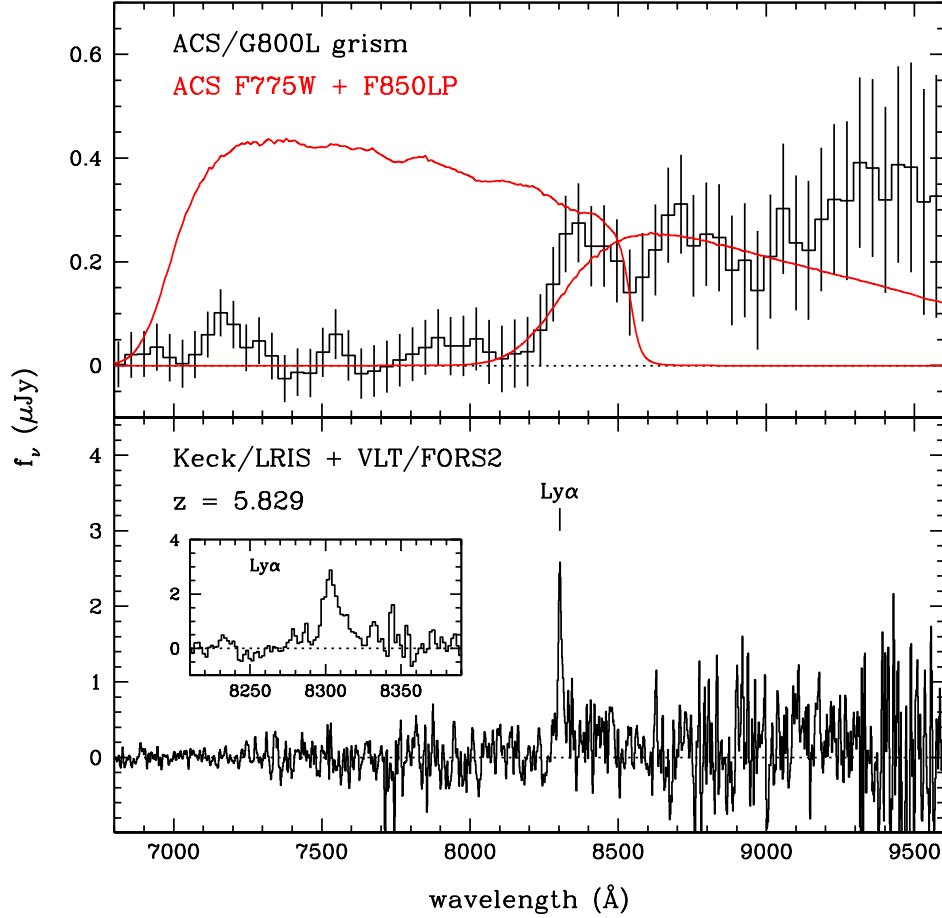


Fig. 2.— (a) *Top*: ACS grism spectrum of SiD2. Pixels in the spectrum are correlated by the data reduction process, and thus have smaller scatter than suggested by the 1σ error bars. Curves show unnormalized bandpass functions for the i_{775} and z_{850} filters. (b) *Bottom*: Keck + VLT spectrum of SiD2, slightly smoothed. The inset panel shows a magnified (unsmoothed) view of the Ly α emission line.

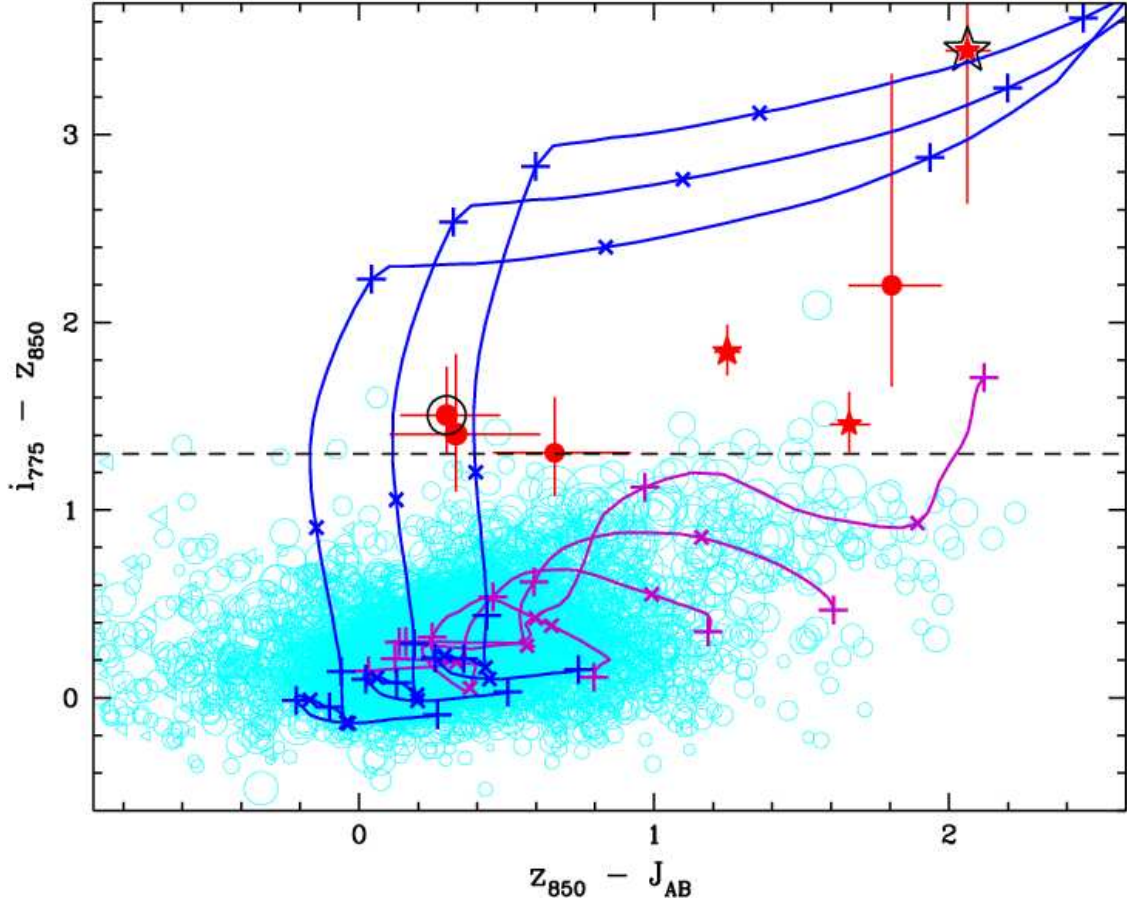


Fig. 3.— Optical–infrared 2-color diagram for the portion of the CDF–S field with deep ISAAC near–IR data. Points show objects with $S/N(z) > 7$, with sizes proportional to their J magnitudes. Filled circles and stars with error bars (1σ) are objects (extended and unresolved) that meet our i –dropout criteria. The point for SiD2 is circled. Open circles show extended objects which do not meet these criteria. Mauve tracks show modeled colors of ordinary, low–redshift galaxies, redshifted over $0 < z < 2$. Blue tracks show expected colors of LBGs at $2 < z < 7$ ($z = 6$ at the “bend”), spanning the range of UV spectral slopes seen in LBGs at $z \approx 3$. Crosses on the tracks mark the same redshifts as in Figure 1.

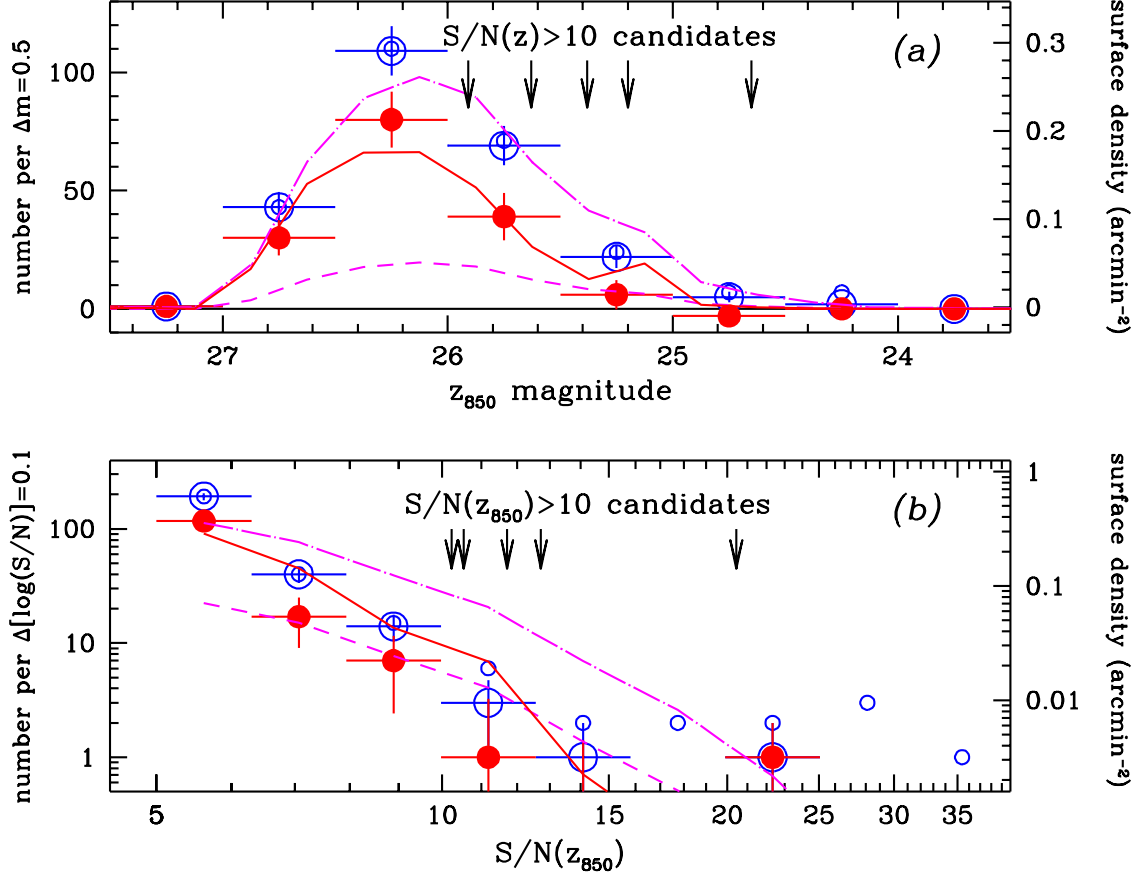


Fig. 4.— Number counts of i -dropout candidates vs. z_{850} magnitude (a) and vs. S/N the z_{850} detection image (b). Small and large open circles show “raw” counts with and without point sources. Filled points are counts after statistical correction for spurious objects. Vertical error bars show \sqrt{N} counting statistics. Arrows indicate locations for the five most secure candidates. Lines show predicted counts from simulations with various assumptions about the galaxy luminosity function. The dot-dashed line uses the $z = 3$ LBG luminosity function, while the short-dashed line uses the same L^* but reduces ϕ^* by a factor of 5. The solid line shows the best-fit Schechter function to the corrected $N(z_{850})$ points, with $L^* = 0.4L_{z=3}^*$ and $\phi^* = 3.8\phi_{z=3}^*$.

Table 1. $z \sim 6$ galaxy candidates, ordered by $S/N(z_{850})^a$

ID	RA (J2000) Dec		$S/N(z_{850})$	$m(z_{850})$	$i_{775} - z_{850}^b$	FWHM(z_{850}) arcsec	Notes
SiD001	03:32:25.60	27:55:48.6	20.45	24.65 ± 0.06	1.63 ± 0.15	0.18	SBM#3 $z = 5.78$ (Bunker et al. 2003)
SiD002	03:32:40.02	27:48:15.0	12.72	25.20 ± 0.12	1.51 ± 0.23	0.19	SBM#1 $z = 5.83$ (this paper); ISAAC
SiD003	03:32:19.07	27:54:21.9	11.72	25.91 ± 0.13	1.39 ± 0.28	0.27	SBM#7; faint IR (SOFI)
NiD001	12:36:19.90	62:09:34.2	10.55	25.63 ± 0.13	> 2.29	0.19	
SiD004	03:32:33.20	27:39:49.2	10.24	25.38 ± 0.13	> 2.21	0.70	faint IR (SOFI)
SiD005	03:32:39.03	27:52:23.1	9.44	25.29 ± 0.17	1.94 ± 0.44	0.28	
SiD006	03:32:45.23	27:49:09.9	9.05	25.91 ± 0.22	1.40 ± 0.31	0.65	
NiD002	12:37:28.62	62:20:39.1	8.79	24.43 ± 0.11	> 2.01	0.77	
SiD007	03:32:42.94	27:52:00.7	8.75	24.97 ± 0.18	1.35 ± 0.30	0.72	
NiD003	12:37:35.90	62:20:43.4	8.67	24.79 ± 0.17	> 1.95	0.93	
SiD008	03:32:13.06	27:49:00.7	8.63	25.78 ± 0.16	1.32 ± 0.31	0.34	
SiD009	03:32:41.36	27:50:04.7	8.58	26.19 ± 0.21	> 2.07	0.14	
SiD010	03:32:26.25	27:48:30.3	8.50	25.41 ± 0.19	1.31 ± 0.26	0.23	ISAAC
NiD004	12:36:42.15	62:09:02.0	8.20	25.55 ± 0.21	1.59 ± 0.52	0.75	
NiD005	12:35:59.01	62:12:45.6	8.15	25.81 ± 0.21	1.55 ± 0.36	0.36	
NiD006	12:36:18.54	62:10:41.9	8.13	26.18 ± 0.17	1.92 ± 0.52	0.28	
NiD007	12:37:52.57	62:17:00.7	8.08	25.93 ± 0.20	> 2.14	0.21	
SiD011	03:32:37.63	27:50:22.4	8.07	25.15 ± 0.21	1.40 ± 0.35	0.88	ISAAC
SiD012	03:32:23.84	27:55:11.5	8.02	26.23 ± 0.18	> 1.98	0.23	
NiD008	12:36:43.53	62:10:04.1	7.89	26.27 ± 0.18	> 1.91	0.19	
NiD009	12:37:12.43	62:18:28.4	7.65	25.94 ± 0.23	> 2.04	0.32	
NiD010	12:36:48.08	62:10:12.6	7.60	25.34 ± 0.22	> 1.80	0.90	
SiD013	03:32:34.69	27:50:22.8	7.57	25.31 ± 0.23	> 1.94	0.87	ISAAC (bright: $J_{AB} = 23.1$, $K_{AB} = 21.6$)
NiD011	12:37:15.75	62:22:32.5	7.43	26.18 ± 0.25	> 1.70	0.13	
NiD012	12:36:48.71	62:12:17.1	7.41	25.37 ± 0.16	1.51 ± 0.34	0.57	
NiD013	12:36:13.04	62:10:43.6	7.34	25.89 ± 0.22	> 1.89	0.58	
NiD014	12:37:22.51	62:18:39.7	7.26	24.23 ± 0.10	1.67 ± 0.50	0.68	
NiD016	12:35:49.72	62:13:29.2	7.21	25.73 ± 0.22	> 1.47	0.61	
NiD015	12:35:50.89	62:11:58.8	7.21	26.02 ± 0.23	1.70 ± 0.52	0.32	
SiD014	03:32:52.22	27:48:04.8	7.20	26.42 ± 0.27	> 1.81	0.25	
NiD017	12:35:52.33	62:12:08.7	7.11	25.23 ± 0.20	1.79 ± 0.55	0.69	
SiD015	03:32:54.11	27:49:16.0	7.06	25.46 ± 0.22	> 1.59	0.47	
SiD016	03:32:11.93	27:41:57.1	7.04	26.38 ± 0.26	1.60 ± 0.50	0.27	
SiD017	03:32:33.16	27:41:17.1	6.95	25.54 ± 0.23	1.76 ± 0.52	0.64	
SiD018	03:32:54.06	27:51:12.0	6.91	26.37 ± 0.21	1.54 ± 0.44	0.19	
SiD019	03:32:36.34	27:43:15.6	6.82	26.18 ± 0.18	> 1.78	0.49	
NiD018	12:36:15.36	62:14:56.4	6.82	25.28 ± 0.15	> 1.76	0.18	
SiD020	03:32:22.27	27:52:57.2	6.80	25.32 ± 0.25	> 2.03	0.68	
SiD021	03:32:25.15	27:48:17.1	6.79	24.79 ± 0.14	> 1.82	0.58	ISAAC
NiD019	12:37:08.89	62:19:19.1	6.78	26.79 ± 0.29	> 1.73	0.15	
NiD020	12:37:35.94	62:14:22.4	6.78	26.16 ± 0.26	> 1.65	0.55	
SiD022	03:32:29.84	27:52:33.2	6.77	26.03 ± 0.22	> 1.72	0.24	
SiD023	03:32:46.05	27:49:29.7	6.75	25.61 ± 0.21	> 1.78	0.32	
NiD022	12:37:12.94	62:18:05.6	6.75	25.71 ± 0.23	> 1.96	0.50	
NiD021	12:36:08.21	62:09:10.8	6.75	26.58 ± 0.21	> 1.84	0.13	
NiD023	12:37:25.35	62:18:45.6	6.70	25.83 ± 0.21	> 1.71	0.41	
NiD024	12:37:42.85	62:19:41.8	6.64	26.37 ± 0.25	> 1.75	0.52	
NiD025	12:36:35.63	62:09:35.8	6.62	26.81 ± 0.22	> 1.46	0.30	

Table 1—Continued

ID	RA (J2000) Dec		$S/N(z_{850})$	$m(z_{850})$	$i_{775} - z_{850}^b$	FWHM(z_{850}) arcsec	Notes
SiD024	03:32:32.46	27:40:02.0	6.56	26.40 ± 0.21	> 1.72	0.30	
NiD026	12:37:34.56	62:20:16.6	6.54	26.32 ± 0.24	> 1.67	0.62	
NiD027	12:35:48.66	62:12:13.3	6.54	25.67 ± 0.28	> 1.72	0.71	
NiD028	12:36:14.37	62:16:17.4	6.53	26.01 ± 0.26	> 1.21	0.21	
NiD029	12:37:32.67	62:14:16.6	6.47	26.28 ± 0.22	> 1.83	0.47	
NiD030	12:35:57.59	62:12:09.2	6.45	25.47 ± 0.21	> 1.68	0.50	
NiD031	12:36:15.08	62:16:34.4	6.41	26.33 ± 0.26	> 1.48	0.50	
SiD025	03:32:36.47	27:46:41.5	6.40	25.76 ± 0.24	> 1.71	0.42	ISAAC
NiD032	12:37:10.96	62:19:48.0	6.39	25.82 ± 0.27	1.62 ± 0.50	0.60	
NiD033	12:37:11.40	62:22:17.0	6.32	26.02 ± 0.24	1.33 ± 0.43	0.42	
NiD034	12:36:45.51	62:18:32.7	6.30	25.86 ± 0.22	> 1.93	0.30	
NiD035	12:36:28.03	62:13:04.8	6.29	25.33 ± 0.25	> 2.00	0.50	
SiD026	03:32:17.25	27:46:46.0	6.27	26.30 ± 0.20	> 1.59	0.22	
NiD037	12:36:50.78	62:20:17.3	6.27	25.87 ± 0.24	> 1.66	0.52	
NiD036	12:37:29.93	62:12:15.4	6.27	26.08 ± 0.25	> 1.50	0.26	
SiD027	03:32:52.52	27:51:44.6	6.26	26.03 ± 0.24	> 1.68	0.57	
NiD038	12:36:27.56	62:13:28.3	6.25	26.24 ± 0.21	> 1.59	0.45	
NiD039	12:36:26.93	62:17:01.2	6.24	25.96 ± 0.23	1.54 ± 0.50	0.41	
SiD028	03:32:16.55	27:41:03.3	6.21	25.93 ± 0.22	1.36 ± 0.45	0.60	
NiD040	12:36:33.20	62:09:23.4	6.20	25.21 ± 0.19	> 1.44	0.70	
NiD041	12:36:49.93	62:08:02.9	6.18	26.86 ± 0.31	> 1.47	0.16	
SiD029	03:32:19.19	27:55:37.9	6.17	25.13 ± 0.21	> 1.51	0.74	
SiD030	03:32:29.33	27:40:14.4	6.16	26.59 ± 0.21	> 1.70	0.17	
SiD031	03:32:56.37	27:53:20.9	6.15	25.53 ± 0.23	> 1.98	0.53	
NiD042	12:36:31.98	62:08:26.3	6.12	26.65 ± 0.23	> 1.76	0.24	
NiD043	12:37:43.01	62:20:02.2	6.09	25.62 ± 0.23	> 1.65	0.57	
NiD044	12:36:48.50	62:10:47.3	6.08	26.28 ± 0.28	> 1.61	0.49	
NiD045	12:36:31.16	62:13:34.0	6.07	25.39 ± 0.30	> 1.84	0.70	
NiD046	12:35:48.97	62:12:25.1	6.07	25.97 ± 0.25	> 1.59	0.27	
NiD047	12:36:26.22	62:11:47.8	6.05	25.91 ± 0.21	> 1.78	0.52	
SiD032	03:32:42.08	27:41:37.2	6.03	26.23 ± 0.29	> 1.51	0.54	
SiD033	03:32:39.45	27:40:26.4	6.02	26.47 ± 0.31	> 1.62	0.39	
NiD048	12:36:28.26	62:08:19.9	5.99	26.40 ± 0.24	> 1.45	0.33	
SiD035	03:32:14.90	27:41:02.7	5.98	26.36 ± 0.30	> 1.72	0.20	
SiD034	03:32:27.39	27:47:28.3	5.98	26.11 ± 0.28	> 1.65	0.49	ISAAC
NiD049	12:36:19.17	62:12:19.6	5.98	25.93 ± 0.31	> 1.73	0.42	
NiD050	12:37:25.65	62:17:43.4	5.97	26.14 ± 0.26	> 1.61	0.50	
NiD052	12:37:37.21	62:19:35.8	5.95	26.76 ± 0.35	> 1.69	0.27	
NiD051	12:37:40.42	62:13:29.5	5.95	25.58 ± 0.26	> 2.06	0.55	
NiD053	12:37:33.19	62:16:42.0	5.94	25.95 ± 0.22	1.43 ± 0.52	0.53	
NiD054	12:37:10.40	62:11:22.1	5.94	26.95 ± 0.26	> 1.57	0.16	
SiD036	03:32:14.75	27:45:41.6	5.92	26.40 ± 0.26	> 1.62	0.24	ISAAC
NiD055	12:36:19.49	62:15:43.3	5.92	26.05 ± 0.25	> 1.58	0.27	
SiD038	03:32:44.70	27:50:02.2	5.90	26.52 ± 0.29	> 1.76	0.29	
SiD037	03:32:22.52	27:56:27.5	5.90	26.25 ± 0.26	> 1.68	0.45	
NiD056	12:37:34.22	62:15:23.2	5.89	26.00 ± 0.28	1.63 ± 0.56	0.56	
NiD057	12:35:47.07	62:12:18.7	5.88	26.50 ± 0.31	> 1.58	0.21	
SiD039	03:32:21.62	27:50:04.4	5.87	25.39 ± 0.25	> 1.61	0.69	ISAAC

Table 1—Continued

ID	RA (J2000) Dec		$S/N(z_{850})$	$m(z_{850})$	$i_{775} - z_{850}^b$	FWHM(z_{850}) arcsec	Notes
NiD058	12:35:53.25	62:10:45.3	5.87	24.99 ± 0.16	1.31 ± 0.46	0.62	
NiD059	12:36:28.86	62:12:22.6	5.86	26.12 ± 0.21	> 1.99	0.22	
NiD060	12:36:10.31	62:10:42.6	5.85	25.93 ± 0.22	> 1.59	0.58	
NiD061	12:36:25.69	62:15:09.5	5.82	26.32 ± 0.26	> 1.68	0.18	
NiD062	12:37:43.82	62:17:26.5	5.80	26.16 ± 0.25	> 1.60	0.47	
NiD064	12:37:17.86	62:18:20.8	5.79	26.17 ± 0.25	> 1.49	0.51	
NiD063	12:36:37.53	62:12:36.3	5.79	26.30 ± 0.25	1.63 ± 0.38	0.43	
NiD065	12:36:58.46	62:21:22.4	5.78	26.40 ± 0.34	> 1.64	0.47	
NiD066	12:37:16.14	62:13:01.0	5.78	25.98 ± 0.25	> 1.59	0.45	
NiD067	12:36:22.71	62:08:37.4	5.77	25.76 ± 0.24	> 1.62	0.39	
NiD068	12:36:48.54	62:18:50.7	5.76	26.09 ± 0.30	> 1.54	0.49	
NiD070	12:36:42.10	62:09:02.4	5.76	26.52 ± 0.30	> 1.27	0.51	
NiD069	12:35:46.99	62:12:28.6	5.76	25.82 ± 0.23	> 1.55	0.45	
NiD071	12:37:01.30	62:21:28.2	5.75	26.36 ± 0.23	1.42 ± 0.50	0.38	
NiD072	12:37:35.60	62:14:45.2	5.75	25.82 ± 0.24	> 1.71	0.42	
NiD074	12:35:56.18	62:11:45.7	5.74	26.18 ± 0.23	1.47 ± 0.53	0.48	
NiD073	12:36:10.32	62:08:10.9	5.74	26.86 ± 0.22	1.31 ± 0.47	0.23	
NiD076	12:37:33.97	62:19:30.5	5.73	26.36 ± 0.24	> 1.62	0.30	
NiD075	12:37:28.86	62:13:21.4	5.73	25.99 ± 0.26	> 1.77	0.23	
NiD077	12:37:38.49	62:19:50.9	5.71	25.96 ± 0.27	> 1.56	0.57	
NiD078	12:36:28.30	62:13:19.7	5.70	25.40 ± 0.22	> 1.87	0.35	
SiD040	03:32:17.95	27:48:16.3	5.68	25.90 ± 0.23	> 1.72	0.28	ISAAC
SiD041	03:32:44.37	27:54:19.1	5.68	25.78 ± 0.23	> 1.61	0.26	
NiD079	12:36:36.34	62:16:49.4	5.68	26.25 ± 0.28	> 1.67	0.14	
NiD082	12:37:37.94	62:19:33.5	5.67	26.03 ± 0.18	> 1.58	0.60	
NiD081	12:36:09.46	62:15:12.6	5.67	26.00 ± 0.27	> 1.50	0.54	
NiD080	12:36:21.37	62:09:23.4	5.67	26.51 ± 0.31	> 1.65	0.42	
SiD042	03:32:22.08	27:42:35.9	5.66	26.32 ± 0.27	> 1.69	0.34	
NiD083	12:37:33.12	62:18:04.6	5.66	26.43 ± 0.24	> 1.55	0.46	
NiD084	12:35:48.44	62:13:04.6	5.66	26.34 ± 0.20	> 1.22	0.49	
SiD043	03:32:50.79	27:47:46.7	5.65	25.97 ± 0.24	> 1.65	0.20	
NiD085	12:37:19.75	62:16:03.1	5.63	25.93 ± 0.25	> 1.63	0.38	
SiD044	03:32:17.78	27:48:13.5	5.62	26.06 ± 0.26	1.63 ± 0.53	0.40	ISAAC
NiD087	12:37:34.18	62:20:55.3	5.60	25.63 ± 0.23	> 1.48	0.56	
NiD086	12:36:46.21	62:18:41.7	5.60	26.36 ± 0.34	> 1.53	0.44	
SiD045	03:32:16.66	27:47:40.0	5.59	26.05 ± 0.22	> 1.46	0.52	ISAAC
NiD089	12:36:49.61	62:10:39.3	5.58	26.01 ± 0.25	> 1.40	0.48	
NiD088	12:35:54.17	62:13:50.4	5.58	26.68 ± 0.26	> 1.16	0.36	
SiD046	03:32:04.52	27:45:55.3	5.55	26.17 ± 0.33	> 1.57	0.53	ISAAC
NiD090	12:37:40.76	62:19:46.3	5.55	25.13 ± 0.20	> 1.55	0.68	
SiD047	03:32:44.47	27:48:21.2	5.54	25.56 ± 0.21	> 1.63	0.32	ISAAC
NiD091	12:36:16.97	62:12:32.5	5.54	26.34 ± 0.29	> 1.53	0.19	
SiD048	03:32:27.89	27:43:15.8	5.53	26.57 ± 0.23	> 1.52	0.30	
NiD092	12:37:09.98	62:12:26.9	5.53	26.24 ± 0.30	> 1.32	0.44	
SiD049	03:32:20.50	27:54:34.6	5.52	26.09 ± 0.25	> 1.34	0.47	
NiD093	12:36:11.20	62:11:07.5	5.52	25.91 ± 0.27	> 1.49	0.55	
SiD050	03:32:53.84	27:51:49.2	5.51	26.12 ± 0.26	> 1.44	0.28	
NiD094	12:36:57.72	62:12:23.9	5.50	26.30 ± 0.24	> 1.54	0.19	

Table 1—Continued

ID	RA (J2000) Dec		$S/N(z_{850})$	$m(z_{850})$	$i_{775} - z_{850}^b$	FWHM(z_{850}) arcsec	Notes
SiD051	03:32:28.34	27:43:15.9	5.49	27.30 ± 0.39	> 1.58	0.17	
NiD095	12:36:57.87	62:19:30.7	5.49	26.44 ± 0.29	> 1.54	0.34	
SiD052	03:32:05.46	27:46:44.2	5.48	26.40 ± 0.26	> 1.41	0.44	
NiD096	12:36:56.99	62:14:05.4	5.48	26.90 ± 0.29	> 1.63	0.23	
SiD055	03:32:34.75	27:40:35.2	5.47	26.65 ± 0.23	> 1.58	0.29	
SiD054	03:32:16.64	27:47:39.6	5.47	26.12 ± 0.24	> 1.45	0.46	ISAAC
SiD053	03:32:35.53	27:53:37.2	5.47	25.72 ± 0.26	> 1.55	0.49	
SiD056	03:32:43.49	27:45:29.2	5.46	26.40 ± 0.29	> 1.46	0.56	
NiD097	12:37:29.90	62:14:08.9	5.46	25.93 ± 0.28	> 1.68	0.49	
NiD099	12:36:45.40	62:18:02.7	5.45	25.70 ± 0.22	> 1.67	0.42	
NiD098	12:37:07.87	62:09:16.9	5.45	26.36 ± 0.28	> 1.28	0.34	
NiD100	12:38:00.87	62:16:11.6	5.44	26.38 ± 0.33	> 1.59	0.43	
NiD102	12:36:57.20	62:10:24.7	5.43	26.29 ± 0.29	> 1.48	0.43	
NiD101	12:36:00.10	62:13:23.6	5.43	26.32 ± 0.29	> 1.54	0.27	
SiD057	03:32:37.96	27:42:07.6	5.42	25.91 ± 0.26	> 1.58	0.24	
SiD058	03:32:54.86	27:48:39.9	5.42	25.68 ± 0.29	> 1.39	0.36	
NiD103	12:37:31.68	62:20:18.7	5.42	25.99 ± 0.29	> 1.46	0.52	
SiD059	03:32:40.70	27:53:26.0	5.41	26.36 ± 0.29	> 1.61	0.40	
NiD104	12:36:58.84	62:10:34.5	5.41	26.60 ± 0.22	> 1.49	0.35	
NiD105	12:36:22.73	62:14:22.0	5.40	26.74 ± 0.29	1.33 ± 0.52	0.26	
NiD106	12:35:45.44	62:12:30.6	5.39	26.50 ± 0.30	> 1.52	0.37	
SiD061	03:32:19.90	27:52:06.1	5.38	26.88 ± 0.26	1.54 ± 0.56	0.26	
SiD060	03:32:36.67	27:54:21.0	5.38	26.65 ± 0.25	> 1.64	0.41	
NiD107	12:36:12.10	62:14:38.1	5.38	25.84 ± 0.23	> 1.53	0.39	
NiD108	12:35:39.26	62:12:29.3	5.38	26.14 ± 0.32	> 1.12	0.36	
NiD109	12:37:09.14	62:22:50.6	5.37	25.69 ± 0.29	> 1.29	0.52	
SiD062	03:32:35.98	27:46:05.1	5.36	26.70 ± 0.41	1.40 ± 0.54	0.29	ISAAC
NiD111	12:36:20.91	62:16:50.8	5.36	26.87 ± 0.40	> 1.63	0.39	
NiD110	12:35:47.37	62:11:33.2	5.36	26.82 ± 0.27	> 1.47	0.37	
SiD063	03:32:22.39	27:48:04.4	5.35	26.64 ± 0.31	> 1.46	0.44	ISAAC
NiD113	12:36:29.26	62:16:31.6	5.35	25.75 ± 0.21	> 1.54	0.38	
NiD112	12:36:22.03	62:15:13.8	5.35	25.83 ± 0.25	> 1.45	0.48	
NiD114	12:36:47.23	62:09:55.5	5.35	26.35 ± 0.29	> 1.43	0.42	
NiD116	12:36:44.51	62:10:28.3	5.34	26.05 ± 0.26	> 1.36	0.49	
NiD115	12:35:57.93	62:13:51.6	5.34	26.17 ± 0.28	> 1.14	0.28	
NiD118	12:37:16.16	62:18:14.9	5.33	26.24 ± 0.26	> 1.52	0.56	
NiD117	12:37:09.62	62:18:14.7	5.33	26.09 ± 0.27	> 1.45	0.60	
NiD119	12:36:12.62	62:13:48.0	5.32	26.37 ± 0.30	> 1.28	0.34	
SiD064	03:32:24.80	27:47:58.8	5.31	26.53 ± 0.29	> 1.54	0.35	ISAAC
SiD065	03:32:40.82	27:47:43.1	5.31	26.32 ± 0.23	> 1.64	0.51	
SiD066	03:32:44.12	27:43:18.4	5.30	25.91 ± 0.27	> 1.49	0.48	
NiD120	12:36:28.07	62:13:19.8	5.30	25.89 ± 0.29	1.50 ± 0.52	0.37	
NiD121	12:37:15.05	62:18:17.8	5.28	25.60 ± 0.23	> 1.46	0.54	
NiD123	12:37:14.84	62:20:15.0	5.27	26.17 ± 0.23	1.40 ± 0.50	0.49	
NiD122	12:36:04.56	62:09:24.7	5.27	26.05 ± 0.27	> 1.43	0.49	
SiD067	03:32:19.46	27:51:59.2	5.26	26.34 ± 0.32	1.34 ± 0.50	0.43	
SiD068	03:32:53.20	27:49:44.3	5.26	26.17 ± 0.27	> 1.53	0.31	
NiD125	12:37:50.65	62:17:22.4	5.26	26.43 ± 0.31	> 1.63	0.40	

Table 1—Continued

ID	RA (J2000) Dec		$S/N(z_{850})$	$m(z_{850})$	$i_{775} - z_{850}^b$	FWHM(z_{850}) arcsec	Notes
NiD124	12:36:37.49	62:16:57.5	5.26	26.57 ± 0.32	> 1.60	0.38	
NiD126	12:36:17.37	62:16:17.7	5.26	26.43 ± 0.30	> 1.41	0.47	
SiD069	03:32:13.06	27:51:33.6	5.25	26.41 ± 0.20	> 1.33	0.26	
SiD070	03:32:39.19	27:54:13.8	5.25	26.55 ± 0.33	> 1.61	0.43	
NiD128	12:36:57.56	62:09:08.5	5.25	25.60 ± 0.24	> 1.38	0.54	
NiD127	12:36:12.41	62:14:49.5	5.25	25.75 ± 0.22	> 1.52	0.45	
SiD071	03:32:14.73	27:47:58.7	5.23	26.12 ± 0.33	1.68 ± 0.47	0.21	ISAAC
SiD072	03:32:47.69	27:46:45.1	5.23	25.13 ± 0.18	> 1.54	0.54	
NiD129	12:37:36.60	62:14:09.7	5.22	26.46 ± 0.25	> 1.62	0.45	
SiD073	03:32:19.05	27:42:44.2	5.21	25.66 ± 0.23	> 1.54	0.51	
NiD130	12:37:31.00	62:19:49.0	5.21	26.37 ± 0.30	> 1.47	0.42	
NiD132	12:37:17.48	62:17:46.3	5.21	25.95 ± 0.26	> 1.49	0.56	
NiD131	12:36:48.78	62:19:39.0	5.21	26.49 ± 0.21	> 1.21	0.45	
SiD074	03:32:34.82	27:51:33.1	5.20	26.32 ± 0.30	> 1.69	0.26	
NiD133	12:37:42.08	62:15:04.4	5.20	25.98 ± 0.26	> 1.53	0.28	
NiD134	12:36:24.96	62:10:56.0	5.20	26.41 ± 0.26	> 1.39	0.23	
NiD136	12:36:51.49	62:20:10.8	5.18	26.88 ± 0.28	> 1.47	0.20	
NiD135	12:36:37.86	62:14:26.8	5.18	26.38 ± 0.20	> 1.44	0.47	
SiD075	03:32:23.88	27:52:04.4	5.17	26.25 ± 0.20	> 1.61	0.43	
NiD137	12:36:27.03	62:11:25.9	5.16	25.81 ± 0.30	> 1.79	0.36	
SiD076	03:32:19.90	27:47:53.2	5.15	25.97 ± 0.28	> 1.41	0.44	ISAAC
SiD077	03:32:21.60	27:44:23.0	5.14	26.60 ± 0.30	> 1.51	0.41	ISAAC
SiD078	03:32:18.54	27:52:59.9	5.14	26.03 ± 0.29	> 1.59	0.51	
NiD139	12:37:39.99	62:20:08.4	5.14	26.93 ± 0.24	> 1.55	0.34	
NiD138	12:37:41.69	62:19:29.4	5.14	26.22 ± 0.23	> 1.47	0.44	
NiD140	12:37:15.31	62:15:35.7	5.14	26.18 ± 0.29	1.47 ± 0.56	0.46	
SiD079	03:32:29.41	27:43:49.4	5.13	26.21 ± 0.28	> 1.49	0.28	
NiD141	12:36:29.43	62:16:44.4	5.13	26.83 ± 0.30	> 1.55	0.29	
NiD144	12:36:41.38	62:17:01.9	5.11	26.76 ± 0.28	> 1.58	0.29	
NiD142	12:37:01.34	62:11:39.7	5.11	25.91 ± 0.26	> 1.43	0.57	
NiD143	12:36:49.09	62:09:12.6	5.11	26.46 ± 0.34	> 1.32	0.46	
SiD080	03:32:18.29	27:48:55.6	5.10	26.63 ± 0.22	1.43 ± 0.58	0.34	ISAAC
SiD082	03:32:16.26	27:44:19.7	5.09	26.68 ± 0.27	> 1.37	0.34	ISAAC
SiD083	03:32:05.13	27:46:40.0	5.09	26.44 ± 0.33	> 1.51	0.30	
SiD081	03:32:52.36	27:48:53.0	5.09	26.19 ± 0.26	> 1.54	0.47	
SiD085	03:32:49.63	27:49:11.1	5.08	26.66 ± 0.34	> 1.52	0.23	
SiD084	03:32:23.37	27:51:55.7	5.08	25.96 ± 0.25	> 1.54	0.27	
NiD145	12:36:50.61	62:10:52.7	5.08	26.58 ± 0.21	> 1.06	0.44	
NiD146	12:36:44.70	62:10:03.1	5.08	26.84 ± 0.27	> 1.45	0.40	
SiD086	03:32:41.17	27:49:47.8	5.06	26.00 ± 0.24	> 1.42	0.34	
SiD088	03:32:39.97	27:41:50.0	5.05	25.89 ± 0.26	> 1.28	0.47	
SiD087	03:32:42.16	27:54:38.8	5.05	25.86 ± 0.27	> 1.53	0.52	
NiD147	12:37:13.52	62:16:20.0	5.05	26.55 ± 0.33	> 1.59	0.34	
SiD089	03:32:29.02	27:42:08.0	5.04	26.94 ± 0.24	> 1.52	0.22	
NiD148	12:36:34.17	62:16:47.1	5.04	26.71 ± 0.25	> 1.55	0.42	
SiD092	03:32:09.91	27:43:36.3	5.03	25.41 ± 0.21	> 1.69	0.50	ISAAC
SiD090	03:32:33.78	27:48:07.6	5.03	26.29 ± 0.30	> 1.49	0.39	ISAAC
SiD091	03:32:49.83	27:48:38.3	5.03	26.40 ± 0.26	> 1.49	0.40	

Table 1—Continued

ID	RA (J2000) Dec		$S/N(z_{850})$	$m(z_{850})$	$i_{775} - z_{850}^b$	FWHM(z_{850}) arcsec	Notes
NiD149	12:37:30.73	62:19:44.7	5.03	26.05 ± 0.27	> 1.42	0.41	
SiD095	03:32:07.57	27:41:30.3	5.02	26.12 ± 0.31	> 1.74	0.39	
SiD093	03:32:21.35	27:50:30.6	5.02	26.46 ± 0.29	1.39 ± 0.51	0.33	ISAAC
SiD094	03:32:21.75	27:50:52.0	5.02	26.32 ± 0.31	> 1.44	0.50	ISAAC
SiD096	03:32:20.72	27:44:35.3	5.01	26.62 ± 0.24	> 1.52	0.42	ISAAC
NiD153	12:36:55.43	62:20:50.5	5.01	26.43 ± 0.30	> 1.38	0.36	
NiD151	12:37:08.17	62:09:42.7	5.01	26.35 ± 0.32	> 1.10	0.41	
NiD154	12:36:29.21	62:13:35.6	5.01	26.80 ± 0.33	> 1.41	0.13	
NiD152	12:36:27.41	62:12:05.3	5.01	25.89 ± 0.29	> 1.75	0.25	
NiD150	12:36:25.29	62:11:41.6	5.01	26.22 ± 0.30	> 1.67	0.39	
NiD155	12:36:24.54	62:15:35.8	5.00	26.93 ± 0.28	> 1.33	0.41	

^aThe robust sample is that with $S/N(z_{850}) > 10$; objects below the line should be regarded with caution, and may include spurious contaminants (see text).

^bColor limits are reported at 2σ